Phase Instability amid Dimensional Crossover in Artificial Oxide Crystal

Seung Gyo Jeong,[1,*] Taewon Min,[2,*] Sungmin Woo,[1] Jiwoong Kim,[2] Yu-Qiao Zhang,[3] Seong Won Cho,[4,5] Jaeseok Son,[6,7] Young-Min Kim,[8,9] Jung Hoon Han,[1] Sungkyun Park,[2] Hu Young Jeong,[10] Hiromichi Ohta,[3] Suyoun Lee,[4] Tae Won Noh,[6,7] Jaekwang Lee,[2,†] and Woo Seok Choi[1,‡]

[1]*Department of Physics, Sungkyunkwan University, Suwon 16419, Korea*
[2]*Department of Physics, Pusan National University, Busan 46241, Korea*
[3]*Research Institute for Electronic Science, Hokkaido University, Sapporo 001-0020, Japan*
[4]*Electronic Materials Research Center, Korea Institute of Science and Technology, Seoul 02792, Korea*
[5]*Department of Materials Science and Engineering, Seoul National University, Seoul 08826, Korea*
[6]*Department of Physics and Astronomy, Seoul National University, Seoul 08826, Korea*
[7]*Center for Correlated Electron Systems, Institute for Basic Science, Seoul 08826, Korea*
[8]*Department of Energy Sciences, Sungkyunkwan University, Suwon 16419, Korea*
[9]*Center for Integrated Nanostructure Physics, Institute for Basic Science, Suwon 16419, Korea*
[10]*UNIST Central Research Facilities and School of Materials Science and Engineering, Ulsan National Institute of Science and Technology, Ulsan 44919, Korea*

(Received 29 July 2019; published 13 January 2020)

Artificial crystals synthesized by atomic-scale epitaxy provide the ability to control the dimensions of the quantum phases and associated phase transitions via precise thickness modulation. In particular, the reduction in dimensionality via quantized control of atomic layers is a powerful approach to revealing hidden electronic and magnetic phases. Here, we demonstrate a dimensionality-controlled and induced metal-insulator transition (MIT) in atomically designed superlattices by synthesizing a genuine two-dimensional (2D) $SrRuO_3$ crystal with highly suppressed charge transfer. The tendency to ferromagnetically align the spins in an $SrRuO_3$ layer diminishes in 2D as the interlayer exchange interaction vanishes, accompanying the 2D localization of electrons. Furthermore, electronic and magnetic instabilities in the two $SrRuO_3$ unit cell layers induce a thermally driven MIT along with a metamagnetic transition.

DOI: 10.1103/PhysRevLett.124.026401

The metal-insulator transition (MIT) is one of the representative phenomena observed in transition metal oxides [1–3]. 3*d* perovskite oxide systems foster MIT, owing to the competition between the itinerant and correlated nature of the charge carriers. For example, $(La, Sr)TiO_3$, $(La, Sr)MnO_3$, and $(La, Sr)CoO_3$ show MIT via charge carrier doping, which alleviates the Mott insulating state. In contrast, $SrVO_3$ and $LaNiO_3$ show a decrease in the bandwidth with decreasing film thickness. On the other hand, MIT is not as common in 4*d* perovskite oxides. Itinerant ferromagnet $SrRuO_3$ (SRO) is one of the 4*d* oxides that exhibits a thickness-dependent MIT. It is known to become insulating as the film thickness decreases below ~4 perovskite unit cells (u.c.) in most cases [4–7]. Experimentally, growth-induced disorder has been predominantly proposed as the origin of the MIT [4,8], while other intrinsic mechanisms, including quantum confinement and orbital ordering, have also been suggested theoretically [9]. In addition, the close relationship between the spin state and electronic structure has been intensively proposed [4,7–10]. Yet, a coherent observation and interpretation of the thickness-dependent MIT is lacking, in part because of the absence of a low-dimensional sample with intrinsic SRO layers.

In the meantime, recent advances in atomic-scale epitaxy have enabled the realization of synthetic crystals with customized dimensions. Indeed, artificial superlattices (SLs) composed of perovskite oxides provide direct access to low-dimensional physical phenomena by manipulating the structural periodicity [11]. Particularly, two-dimensional electron liquids have been intensively studied in terms of quantum confinement, resonant tunneling, and thermopower enhancement [12–14]. Such unprecedented capability lets us explore the fundamental aspects of MIT in low dimensions.

In this Letter, we report an intrinsic MIT in SRO with electronic interfaces as sharp as atomic interfaces. A close correlation between the electronic structure, transport properties, and spin ordering is revealed, which is strongly dependent on the system dimensions. Thus, the 3 u.c. layer of SRO is ferromagnetic metallic (FMM), while the 1 u.c. one is antiferromagnetic insulating (AFMI). Furthermore, a phase instability is observed for the SRO layer with 2 u.c. thickness, which bridges the two- and three-dimensional states. Herein, a thermally driven MIT with strongly coupled magnetic ordering is found, manifesting the dimensional instability between the FMM and AFMI phases. Our results describe the evolution of the strongly

coupled electronic and magnetic phases via atomic-scale-dimensional engineering of correlated materials.

Customization of the dimension of the SRO crystals was achieved by systematically controlling the number of atomic unit cell layers of SRO and $SrTiO_3$ in $[(SRO)_x|(STO)_y]_{10}$ ($x(y)$ unit cell layers of SRO (STO) repeated ten times along the growth direction $[x|y]$) SLs using pulsed laser deposition (PLD) (Figs. S2–S4 and Supplemental Material Secs. 1 and 2 [15]). We note that the epitaxial strain can modify the electromagnetic properties of SRO [33]. However, all the SRO-STO SLs shown here are coherently strained to the STO substrate [Fig. S4(b)], negating the degree of strain as a control parameter. The absence of charge transfer across the SRO-STO interface was confirmed from optical spectroscopy, which suggest that the SRO-STO SLs embody intrinsic SRO layers. Figure 1(a) shows the optical conductivity spectra $[\sigma_1(\omega)]$ of the SLs with varying periodicity. The increase in $\sigma_1(\omega)$ below ~1 eV for most of the SLs manifest the Drude contribution, reflecting the metallic nature. Notably, an isosbesticlike point appears at ~3.86 eV, indicating that the optical sum rule is obeyed for the SL systems. The spectral weight is exchanged across the reference point of the isosbesticlike point at which the values of optical conductivity are the same for bare SRO and STO. Indeed, the total optical spectral weight (SW) of the SRO-STO SLs changes *linearly* as a function of the $x/(x+y)$ volume ratio of the SRO layer, as shown in Fig. 1(b). Moreover, the SWs below and above the isosbestic point are linearly exchanged with each other, suggesting that $\sigma_1(\omega)s$ of the SLs can be simply constructed from a linear combination of the $\sigma_1(\omega)s$ of the individual SRO and STO layers. [Note that the total SW increases slightly with $x/(x+y)$ because $\sigma_1(\omega)$ was measured only up to ~5.5 eV, such that the contribution from the higher energy tail is excluded.] The absence of contributions from the interfacial electronic state indicates the suppression of charge transfer across the interface between SRO and STO (Fig. S5 and Supplemental Material Sec. 3 [15]).

In general, the electronic density profile at the interface is broader than the chemical interface due to the prevailing charge transfer at the isostructural perovskite oxide heterointerfaces [34]. While polar discontinuity is a prominent example of the electronic reconstruction of the interface between a polar and a nonpolar material [35], even some nonpolar materials can form an interface with a substantial charge transfer manifesting the strong covalent or ionic bonding in the oxides [36]. Recently, Zhong and Hansmann proposed a band alignment scheme to quantitatively estimate the charge transfer at the complex oxide interfaces [37]. The misalignment of oxygen p bands across the heterointerface can yield a Fermi energy mismatch, which might lead to an electron transfer across the interface. According to their results, a small Fermi energy mismatch between SRO and STO can result in an interface with highly suppressed charge transfer. Our first-principles density functional theory (DFT) calculations support the existence of an atomically sharp-electronic-interface, as the layered density of states (LDOS) has no defect or interface states associated with charge transfer [Fig. 1(d)]. Therefore, an intrinsic 2D SRO system is realized through the SRO-STO SLs.

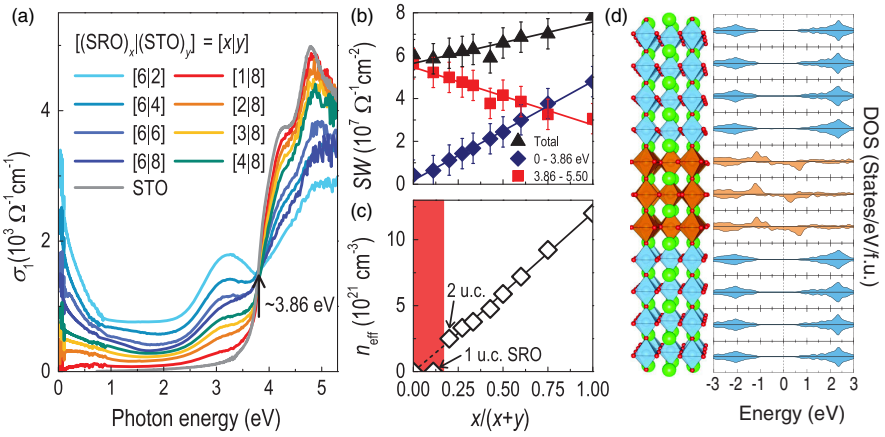

FIG. 1. Absence of electronic reconstruction in SRO-STO SLs. (a) $\sigma_1(\omega)$ of $[(SRO)_x|(STO)_y]_{10}$ ($[x|y]$) SLs. The ratio between the thicknesses of the SRO and STO layers systematically influence $\sigma_1(\omega)$ of the SLs, with the appearance of an isosbesticlike point at ~3.86 eV. (b) The W_s of the low energy region (0.04–3.86 eV, blue rhombus) increases linearly with increasing volume (thickness) the fraction of the SRO layer, whereas the W_s of the high energy region (3.86–5.5 eV, red square) decreases linearly. The total W_s is indicated by the black triangles. (c) Effective carrier concentration (n_{eff}) of SLs calculated from the Drude contribution of $\sigma_1(\omega)$. A clear MIT is observed for the $x = 1$ SL with an abrupt disappearance of the Drude peak in $\sigma_1(\omega)$ and the resulting n_{eff}. The regions in red indicate the insulating phase. (d) The layered density of states (LDOS) of the [3|8] SL does not show any defect or interface states, indicating the absence of the electronic reconstruction. Blue (orange) colored layers are the LDOS from the STO (SRO) layers. The vertical dashed line indicates the Fermi energy level.

The atomically sharp-electronic-interface pushes the thickness limit of metallicity in SRO down to 2 u.c. The metallicity of SRO was quantitatively characterized by the effective carrier concentration (n_{eff}) obtained from the Drude model in $\sigma_1(\omega)$ [Figs. 1(c) and Supplemental Material Sec. 4 [15]]. The linear behavior of n_{eff} as a function of $x/(x+y)$ again suggests the absence of the charge transfer across the interface and indicates that the metallicity of the SRO is well maintained to $x = 2$. The metallic behavior abruptly disappeared at $x = 1$ SL with a gap opening ($E_g \sim 30$ meV) [Fig. 1(a)], manifesting the dimensionality-induced MIT.

dc electrical transport confirmed the MIT at $x = 1$ SL [Fig. 2(a)], which is consistent with the optical spectra. In contrast to the previous studies [4,5], the temperature-dependent electrical resistivity [$\rho(T)$] well preserves the intrinsic metallic nature of SRO down to 2 u.c. This is due to the elimination of extrinsic factors such as surface structural-electronic reconstruction and/or disorder in the layers (Figs. S6, S7, and Supplemental Material Sec. 5 [15]). The $\rho(T)$ curve shows an insulating behavior only for the $x = 1$ SL. The activation gap was estimated to be ~20 meV (Fig. S8), which is similar to the optical gap. Thermopower [$S(T)$] measurements for the SLs also showed a clear distinction between the metallic ($x \geq 2$) and insulating ($x = 1$) SLs. As shown in Fig. 2(b), a large suppression of hole carriers in the $x = 1$ SL led to a drastic increase in the thermopower, resembling the behavior of conventional semiconductors (Supplemental Material Sec. 6 [15]).

As the metallicity disappears at the 2D limit of the SRO layers, the spin-ordered state undergoes a concomitant change. Figure 2(c) shows the field-cooled (FC) temperature-dependent magnetization [$M(T)$]. The conventional ferromagnetism of the SRO layers is systematically suppressed, with a decrease in the FM transition temperature T_c, as x decreases [inset of Fig. 2(c)] [38]. When x becomes one, the FM behavior completely disappears over the entire

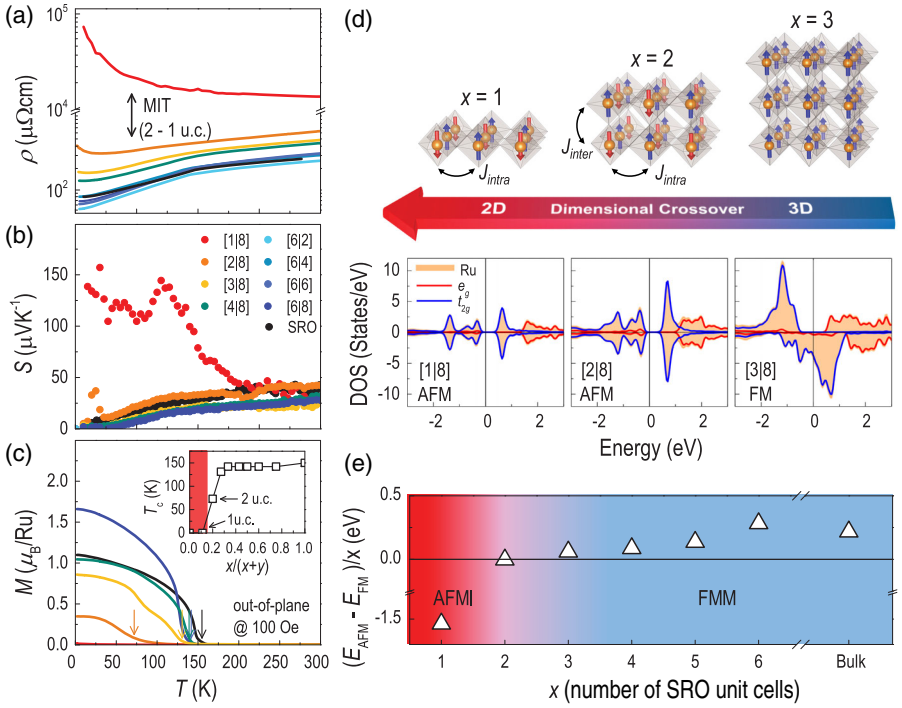

FIG. 2. Dimensional crossover of electrical transport and magnetic properties. (a) $\rho(T)$ of the $[x|y]$ SLs maintain their metallic behavior down to $x = 2$. A clear MIT is observed for the $x = 1$ SL, consistent with the optical results. (b) $S(T)$ of the SLs shows hole-dominant electrical transport originating from the SRO layers. The $x = 1$ SL shows significantly enhanced $S(T)$ values resembling the behavior of semiconductors with bipolar conduction. (c) $M(T)$ are shown for the SLs, indicating ferromagnetic transitions at low temperature. The arrows indicate the FM T_c of the SLs. The inset shows T_c as a function of the SRO fraction within the SLs. Ferromagnetic (FM) ordering of the SRO vanishes for the $x = 1$ SL, concomitant with the MIT. The $M(T)$ curves were measured under 100 Oe of the magnetic field along the out-of-plane direction of the thin films. (d) Upper panel: Schematic representation of the spin ordering transition of SRO across the dimensional crossover from 3D to 2D. J_{intra} and J_{inter} represent magnetic exchange coupling along and across the layers, respectively. Lower panel: DOS obtained by DFT calculations of $[x|8]$ ($x = 1$, 2, and 3) SLs, reproducing the experimentally observed magnetically coupled MIT. The magnetic phase transition from FMM ($x = 3$) to AFMI ($x = 1$) is shown, with the appearance of dimensional instability for the $x = 2$ SL. (e) The calculated energy difference between AFM and FM magnetic configurations as a function of SRO atomic unit cell thickness, where the energy difference is normalized by the SRO thickness. The red (blue) region indicates the AFMI (FMM) phase.

temperature range, suggesting a dimensionality-induced transition from a FM to an AFM or paramagnetic state. This magnetic phase transition at $x = 1$ SL coincides with the dimensional crossover of the electronic state observed by optical and electronic transport measurements. DFT calculations provide further insight into this magnetically coupled MIT (Fig. S9). Figure 2(d) shows the density of states (DOS) of the SLs with $x = 1$, 2, and 3. $x = 1$ and 2 SLs show an AFMI phase, with a band gap between the d_{xy} and $d_{yz,zx}$ of the Ru$-t_{2g}$ orbitals corresponding to the crystal field splitting (Fig. S10) [9]. In contrast, $x = 3$ SL shows an FMM phase with a closed gap and spin-polarized DOS, wherein the t_{2g} orbitals are more or less uniformly occupied (Fig. S10). The dimensionality-induced magnetic and electronic phase transition can, therefore, be interpreted as an anisotropic hybridization of the Ru$-t_{2g}$ orbitals at low dimension. In particular, the low-dimensional SRO layer breaks the crystalline periodicity at the interfaces by eliminating the Ru-O orbital hybridization along the out-of-plane direction. As a result, the d_{xy} orbital becomes lower in energy than the $d_{yz/zx}$ orbitals, resulting in an effective half-filled system [39]. The highly anisotropic hybridization naturally implies the strongly coupled magnetic and electronic states via anisotropic magnetic exchange interaction [40]. As schematically shown in Fig. 2(d), the interlayer exchange interaction J_{inter} naturally vanishes for the $x = 1$ SL, stabilizing the AFMI phase.

The theoretical calculation correctly captures the qualitative nature of the dimensionality-induced MIT strongly coupled to the spin ordering, yet, an apparent discrepancy seems to exist. For the DFT calculation, the MIT occurs at $x = 2$, whereas it occurs at $x = 1$ for the experiment. However, a closer inspection of the $x = 2$ SL shows that the theoretical calculation turns out to be in excellent agreement with the experiment, especially considering that the DFT calculation is performed at 0 K. Specifically, the x-dependent total energy difference [Fig. 2(e)] shows that the AFM and FM configurations have nearly degenerate energy for $x = 2$ SL (Fig. S9). The AFM configuration is only $\sim$5 meV$/f$.u. lower in energy than the FM one, reflecting the phase instability. Thus, one might experimentally expect an AFMI ground state when the temperature is lowered.

Figure 3 shows an intriguing temperature-dependent magnetic instability for the $x = 2$ SL, capturing the phase instability amid the dimensional crossover. Particularly, a broad first-order-like phase transition was observed around 40 K (T^*) in the zero-field-cooled (ZFC) measurement [Fig. 3(a)]. Figures 3(b) and 3(c) further show that an intriguing temperature-dependent MIT occurred below $\sim$40 K (T_{MIT}), with a clear upturn in $\rho(T)$ accompanied by an anomaly in $S(T)$. T_{MIT} synchronized with T^* of the magnetic phase transition for $x = 2$ SL, again indicating that the magnetic and electronic degrees of freedom are strongly coupled. Note that this temperature scale also

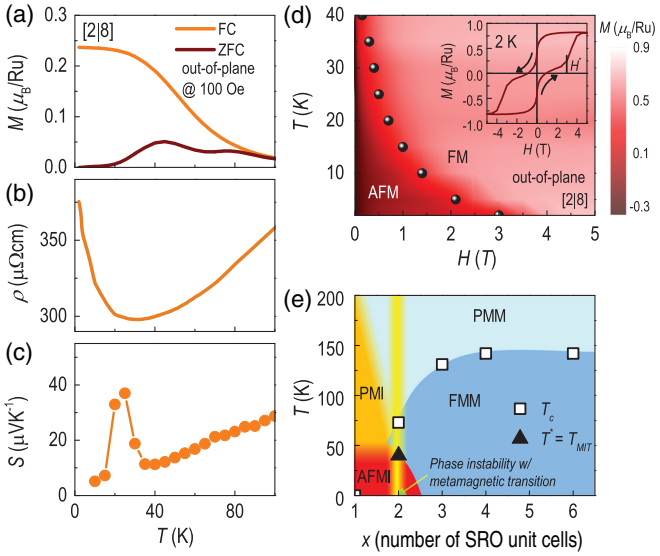

FIG. 3. Dimensional phase evolution and instability of the atomically designed SRO-STO SLs. (a)–(c) Dimensional instability in $x = 2$ SL is evidenced by a thermally induced phase transition occurring simultaneously for the electronic and magnetic structures at $\sim$40 K (T_{MIT}). (a) Although FC $M(T)$ shows a single ferromagnetic transition at $\sim$75 K, ZFC $M(T)$ shows a secondary magnetic transition. We applied 100 Oe of the magnetic field along the out-of-plane direction of the thin film. (b) $\rho(T)$ and (c) $S(T)$ indicate that this magnetic transition accompanies the transition to an insulating phase below the T_{MIT}. (d) A temperature-magnetic field phase diagram of $x = 2$ SL was plotted from $M(H)$ curves. The data points indicate the magnetic field (H^*) required for the metamagnetic transition at different temperatures. The inset shows the magnetic hysteresis behavior of $x = 2$ SL at 2 K. The arrows of the inset indicate the field directions. (e) Phase diagram as a function of SRO thickness and temperature constructed from the experimental and theoretical results, highlighting the dimensionality-induced phase transition and phase instability across the dimensional crossover. The empty squares and solid triangles indicate the T_c and $T^* = T_{\text{MIT}}$, respectively. The light blue, blue, yellow, and red regions denote PMM, FMM, PMI, and AFMI phases, respectively.

coincides with the total energy difference obtained between the AFM and FM configurations from the DFT calculation, which can be converted to a temperature of $\sim$25.8 K, close to the T^* and T_{MIT} (Supplemental Material Sec. 7 [15]).

The nature of the phase transition for $x = 2$ SL can be better perceived from the magnetic-field dependence as shown in Fig. S11 and the inset of Fig. 3(d). Whereas $M(H)$ curves below T_c show typical ferromagnetic hysteresis loops for the SRO thin film, they evolve into a double hysteresis loop as the temperature is further lowered below T^*. The possible spin configurations associated with the appearance of the double hysteresis loop are interlayer exchange coupling [41], FM-AFM [42], or FM-FM [43] heterostructures with different coercivity, structural distortions, and metamagnetic transition [44–48]. We first rule out the interlayer exchange coupling for the $x = 2$ SL by

showing a similar $M(H)$ curve for the [2|18] SL with a large enough STO spacer thickness (Fig. S12). Second, in order for the FM-AFM or FM-FM heterostructures to exhibit double hysteresis, exchange bias should always exist [47], which is not our case. Third, we used structural analyses [Fig. S4(c)] to rule out any anomalous structural distortion in [2|y] SLs. The last candidate, i.e., the metamagnetic transition, is the most probable. Indeed, a double hysteresis can originate from a field-induced first order metamagnetic transition above a finite magnetic field ($>H^*$) at low temperature ($<T^*$) [46,48]. Magnetoresistance (MR) measurements support the metamagnetic transition based on the closely coupled electronic phase and spin ordering in $x = 2$ SL (Fig. S13). A typical MR behavior of SRO shows a sharp peak at the coercive field (H_c) with a negative MR above H_c [49]. However, in the $x = 2$ SL, $\rho(H)$ shows a rather broad maximum below H^* as shown in Fig. S13, indicating an AFMI phase (Supplemental Material Sec. 8 [15]). $\rho(H)$ decreased with increasing H only when the FMM phase was above H^*.

The metamagnetic transition in the $x = 2$ SL is summarized in Fig. 3(d) as a function of H and T. A similar magnetic transition accompanying the MIT was observed in manganites with colossal magnetoresistance [48], but the origin is fundamentally different from the SRO systems without any charge ordering. It is also interesting to compare $x = 2$ SL with the natural crystal of layered perovskite $Sr_3Ru_2O_7$, since both possess a close structural similarity considering the two RuO_6 octahedral layers. While $Sr_3Ru_2O_7$ does not show an MIT, it does undergo a metamagnetic transition. The metamagnetic transition occurs at a higher magnetic field (>7 T), possibly owing to the different strain state on the SRO layers or chemical environment. Despite these distinctions, it is likely that the dimensional instability plays an important role in inducing the metamagnetic transitions in both materials. A temperature-thickness phase diagram was constructed to synopsize the phases of the low-dimensional SRO [Fig. 3(e)]. It summarizes how the typical FMM evolves into an AFMI phase in the 2D limit and indicates the dimensional instability in between.

In conclusion, we have observed the intrinsic MIT of SRO via the dimensional crossover in atomically designed SRO-STO SLs. A clear dimensionality-induced MIT was observed, strongly coupled to the magnetic ordering. For the 2 u.c. SRO layers, a phase amid the dimensional crossover was discovered manifested by a temperature-dependent electronic and magnetic phase transition. The result underscores the dimensional instability which can be further extended to general strongly correlated systems.

We are grateful for insightful discussions with Lingfei Wang, Ambrose Seo, and Jong Mok Ok. This work was supported by the Basic Science Research Programs through the National Research Foundation of Korea (NRF) (No. NRF-2019R1A2B5B02004546). J. L. and Y.-M. K. were supported by the Samsung Research Funding & Incubation Center of Samsung Electronics (No. SRFC-MA1702-01). S. W. C and S. L. were supported by NRF (No. NRF-2019M3F3A1A02072175). J. S. and T. W. N. were supported by the Institute for Basic Science (No. IBS-R009-D1). Y.-M. K. was supported by the IBS (No. IBS-R011-D1) and Creative Materials Discovery Program (No. NRF-2015M3D1A1070672). J. H. H. was supported by the Samsung Science and Technology Foundation (No. SSTF-BA1701-07). H. O. was supported by Grants-in-Aid for Scientific Research A (17H01314) and Innovative Areas (19H05791) from the Japan Society for the Promotion of Science, and the Cooperative Research Program of the "Network Joint Research Center for Materials and Devices: Dynamic Alliance for Open Innovation Bridging Human, Environment and Materials".

*S. G. J. and T. M. contributed equally to this work.
†jaekwangl@pusan.ac.kr
‡choiws@skku.edu

[1] M. Imada, A. Fujimori, and Y. Tokura, Rev. Mod. Phys. **70**, 1039 (1998).
[2] R. G. Moore, J. Zhang, V. B. Nascimento, R. Jin, J. Guo, G. T. Wang, Z. Fang, D. Mandrus, and E. W. Plummer, Science **318**, 615 (2007).
[3] P. D. C. King, H. I. Wei, Y. F. Nie, M. Uchida, C. Adamo, S. Zhu, X. He, I. Božović, D. G. Schlom, and K. M. Shen, Nat. Nanotechnol. **9**, 443 (2014).
[4] J. Xia, W. Siemons, G. Koster, M. R. Beasley, and A. Kapitulnik, Phys. Rev. B **79**, 140407(R) (2009).
[5] S. Kang *et al.*, Phys. Rev. B **99**, 045113 (2019).
[6] H. Boschker *et al.*, Phys. Rev. X **9**, 011027 (2019).
[7] H. Jeong, S. G. Jeong, A. Y. Mohamed, M. Lee, W.-s. Noh, Y. Kim, J.-S. Bae, W. S. Choi, and D.-Y. Cho, Appl. Phys. Lett. **115**, 092906 (2019).
[8] Y. J. Chang, C. H. Kim, S. H. Phark, Y. S. Kim, J. Yu, and T. W. Noh, Phys. Rev. Lett. **103**, 057201 (2009).
[9] S. Ryee and M. J. Han, Sci. Rep. **7**, 4635 (2017).
[10] P. Mahadevan, F. Aryasetiawan, A. Janotti, and T. Sasaki, Phys. Rev. B **80**, 035106 (2009).
[11] R. Ramesh and D. G. Schlom, Nat. Rev. Mater. **4**, 257 (2019).
[12] K. Yoshimatsu, K. Horiba, H. Kumigashira, T. Yoshida, A. Fujimori, and M. Oshima, Science **333**, 319 (2011).
[13] W. S. Choi, S. A. Lee, J. H. You, S. Lee, and H. N. Lee, Nat. Commun. **6**, 7424 (2015).
[14] H. Ohta *et al.*, Nat. Mater. **6**, 129 (2007).
[15] See Supplemental Material at http://link.aps.org/supplemental/10.1103/PhysRevLett.124.026401 for (1) methods, (2) atomically designed SRO/STO SLs, (3) effective medium approximation, (4) obtaining effective carrier density from $\sigma_1(\omega)$, (5) thickness-dependent resistivity of SRO, (6) thermopower analysis of MIT, and (7) Néel temperature calculation for 2 u.c. of SRO, and (8) magnetic ground state of $x = 2$ SL, which includes Refs. [16–32].
[16] P. E. Blöchl, Phys. Rev. B **50**, 17953 (1994).

[17] G. Kresse and J. Furthmüller, Comput. Mater. Sci. **6**, 15 (1996).
[18] W. Cai and V. Shalaev, *Optical Metamaterials: Fundamentals and Applications* (Springer, Heidelberg, Germany, 2009).
[19] K. W. Kim, J. S. Lee, T. W. Noh, S. R. Lee, and K. Char, Phys. Rev. B **71**, 125104 (2005).
[20] C. S. Alexander, S. McCall, P. Schlottmann, J. E. Crow, and G. Cao, Phys. Rev. B **72**, 024415 (2005).
[21] F. Bern, M. Ziese, A. Setzer, E. Pippel, D. Hesse, and I. Vrejoiu, J. Phys. Condens. Matter **25**, 496003 (2013).
[22] K. Ueda, H. Saeki, H. Tabata, and T. Kawai, Solid State Commun. **116**, 221 (2000).
[23] Z. Liu *et al.*, Appl. Phys. Lett. **101**, 223105 (2012).
[24] M. Izumi, K. Nakazawa, and Y. Bando, J. Phys. Soc. Jpn. **67**, 651 (1998).
[25] C. Kittel and P. McEuen, *Introduction to Solid State Physics* (Wiley, New Jersey, 1996).
[26] M. Jonson and G. D. Mahan, Phys. Rev. B **21**, 4223 (1980).
[27] C. Berglund and H. Guggenheim, Phys. Rev. **185**, 1022 (1969).
[28] E. S. Toberer, C. A. Cox, S. R. Brown, T. Ikeda, A. F. May, S. M. Kauzlarich, and G. J. Snyder, Adv. Funct. Mater. **18**, 2795 (2008).
[29] D. Fu, K. Liu, T. Tao, K. Lo, C. Cheng, B. Liu, R. Zhang, H. A. Bechtel, and J. Wu, J. Appl. Phys. **113**, 043707 (2013).
[30] T. Katase, K. Endo, and H. Ohta, Phys. Rev. B **92**, 035302 (2015).
[31] Y. Klein, S. Hébert, A. Maignan, S. Kolesnik, T. Maxwell, and B. Dabrowski, Phys. Rev. B **73**, 052412 (2006).
[32] G. Fischer, M. Däne, A. Ernst, P. Bruno, M. Lüders, Z. Szotek, W. Temmerman, and W. Hergert, Phys. Rev. B **80**, 014408 (2009).
[33] Q. Gan, R. A. Rao, C. B. Eom, J. L. Garrett, and M. Lee, Appl. Phys. Lett. **72**, 978 (1998).
[34] A. Ohtomo, D. A. Muller, J. L. Grazul, and H. Y. Hwang, Nature (London) **419**, 378 (2002).
[35] N. Nakagawa, H. Y. Hwang, and D. A. Muller, Nat. Mater. **5**, 204 (2006).
[36] L. Chen, J. Li, Y. Tang, Y.-Y. Pai, Y. Chen, N. Pryds, P. Irvin, and J. Levy, Adv. Mater. **30**, 1801794 (2018).
[37] Z. Zhong and P. Hansmann, Phys. Rev. X **7**, 011023 (2017).
[38] M. Izumi *et al.*, Solid State Ionics **108**, 227 (1998).
[39] A. Liebsch and H. Ishida, Phys. Rev. Lett. **98**, 216403 (2007).
[40] T. Song *et al.*, Science **360**, 1214 (2018).
[41] B. Chen *et al.*, Science **357**, 191 (2017).
[42] X. Ning, Z. Wang, and Z. Zhang, J. Phys. D **46**, 452001 (2013).
[43] Q. Qin, W. Song, S. He, P. Yang, and J. Chen, J. Phys. D **50**, 215002 (2017).
[44] E. Stryjewski and N. Giordano, Adv. Phys. **26**, 487 (1977).
[45] R. S. Perry *et al.*, Phys. Rev. Lett. **86**, 2661 (2001).
[46] K. J. Singh, S. Chaudhary, M. K. Chattopadhyay, M. A. Manekar, S. B. Roy, and P. Chaddah, Phys. Rev. B **65**, 094419 (2002).
[47] J. Nogués and I. K. Schuller, J. Magn. Magn. Mater. **192**, 203 (1999).
[48] H. Kuwahara, Y. Tomioka, A. Asamitsu, Y. Moritomo, and Y. Tokura, Science **270**, 961 (1995).
[49] M. Bibes, B. Martinez, J. Fontcuberta, V. Trtik, F. Benitez, C. Ferrater, F. Sanchez, and M. Varela, Phys. Rev. B **60**, 9579 (1999).